Advances in Science and Technology Research Journal

Advances in Science and Technology Research Journal, 2026, 20(2), 402–416
https://doi.org/10.12913/22998624/211975
ISSN 2299-8624, License CC-BY 4.0

Received: 2025.09.14
Accepted: 2025.12.15
Published: 2025.12.23

Dynamic response of the steel roof covering to strong gusts of foehn wind

Urszula Radoń[1], Paweł Zabojszcza[2*], Waldemar Szaniec[3]

[1] Faculty of Civil Engineering and Architecture, Kielce University of Technology, 25-314 Kielce, Poland
* Corresponding author's e-mail: pawelzab@tu.kielce.pl

ABSTRACT

This study examined the dynamic response of a steel roof covering subjected to strong foehn wind gusts. Since this is not a standard design scenario, a static analysis of wind-loaded structures alone is insufficient. The paper incorporated inertia forces and dynamic equilibrium equations. The equations of motion are calculated an unconditionally stable version of the Newmark method. Numerical simulations were conducted using novel MES3D program. Wind speed was modelled according to the Kaimal spectrum. Modal and spectral analyses were performed for average wind speeds of 30, 35 and 40 m/s to identify the frequencies that may induce resonance. The study determined the displacements, accelerations, and axial forces of the steel roof covering.

Keywords: dynamic response, spectral analysis of signals, modal analysis, Newmark method.

INTRODUCTION

In mountainous terrain, such as Zakopane and the surrounding Tatra Mountains, winds behave differently than in lowland areas. These changes are the result of complex terrain, altitude differences, and local meteorological phenomena. The foehn wind is one of the most characteristic and powerful meteorological phenomena occurring in the Tatra Mountains, especially on the Polish side – in Zakopane and surrounding towns. Its presence clearly affects the climate, the natural environment, and the well-being of people. The foehn wind is a local dry, warm, and gusty wind blowing from the mountains towards the valleys. In [1], the author identified the most common types of synoptic situations favouring the foehn and compared them with statistics of days with its occurrence. The article also demonstrated the seasonality of the phenomenon and indicated that the foehn most often occurs as a result of the presence of a low pressure over Western Europe and a high pressure over Russia. [2] did not analyse the foehn phenomenon in as much detail as [1], but it provided an important contextual source. Key to the foehn wind are the maps showing the frequency of strong winds and local air circulation patterns in mountainous regions. The atlas also provides data on the impact of terrain on airflow. Temperatures during the foehn wind can rise by several, or even a dozen, degrees Celsius within a few hours. Humidity drops significantly, and the air becomes dry and "rough". The foehn wind in the Tatra Mountains is characterised by strong gusts, often exceeding 30–40 m/s. In Zakopane, gusts of over 140 km/h were recorded in December 2013. The foehn wind felled hundreds of trees, caused power outages, and ripped off dozens of roof coverings. Within a few hours, the temperature rose by 10 °C.

Engineers use wind tunnel tests and CFD simulations to thoroughly understand the distribution of wind forces on the surface of domes. This allows them to assess how the dome reacts to various wind conditions, including hurricanes and tornadoes. Sun, Qiu, Wu [3] estimated the wind pressure spectrum characteristics for twelve models of spherical dome roofs with different geometric parameters (rise/span and

height/span ratios) based on a series of tests in a wind tunnel. They obtained a synthetic spectral model of the wind loading. As a result of their experiment, they proposed a spectral model of wind pressure which can be utilised for the extreme and fatigue design of structural roofs. Ren et al. [4] analysed the wind vibration coefficient and the most critical part of wind-induced vibrations in a large-span thin dome structure using the finite element method for three-dimensional time-domain wind vibration analysis. The wind load was simulated using the harmonic superposition method, obtaining a time-varying wind velocity curve and a time-varying wind pressure curve. The influence of the dome thickness was taken into account in the analysis of vibration coefficient changes. The results showed that the wind coefficient of the large-span dome structure increased with decreasing thickness, and its central part was the most critical region for wind-induced vibrations. Tavares in his work [5] proposed parametric modelling of the distribution of wind loads on a hemi-spherical dome surface. On the basis of a combination of wind speed, internal and external pressure coefficients, building dimensions, topography, and terrain roughness, he determined the magnitude and direction of a field of distributed normal forces on the surface of the analysed dome. Szmit [6] presented the results of a static analysis of selected geodesic domes subjected to their self-weight and wind load. The calculations were performed on geodesic domes based on an octahedron and icosahedron, depending on the density of the geodesic division. The results showed that the maximum vertical displacements of the structure vertices due to wind load were in accordance with applicable standards and approximately 10% lower than those obtained from experimental tests. However, the author suggested that for structures with large spans, wind tunnel tests should be conducted due to the fact that the distributions of the external pressure coefficient at different Reynolds numbers can significantly deviate from the distribution assumed in Eurocode or American standards. Khosrowjerdi et al. [7] conducted numerical analyses using computational fluid dynamics (CFD) to investigate changes in the wind pressure coefficient Cp at various heights and angles on 15 Iranian buildings with domed roofs. On the basis of the obtained results, they identified the appropriate dome shapes, which significantly influences the wind loading magnitude. The presented studies provide comprehensive information, but they have a fundamental disadvantage. This disadvantage is their price. Additionally, using CFD software requires specialist knowledge that the average designer does not have. An alternative in this situation are numerical simulations. This is the path chosen by the authors of this article.

This study investigated the dynamic response of a steel bar roof in the form of a Schwedler dome subjected to strong foehn wind gusts. Such wind action is not typically considered in standard design scenarios; therefore, a purely static analysis of wind-loaded structures proves insufficient. In order to capture the essential effects, the study incorporated inertia forces and the full dynamic equilibrium equations of motion, solved using an unconditionally stable variant of the Newmark method. Numerical simulations were carried out with the novel proprietary MES3D program, which enables detailed analysis of spatial bar structures under complex dynamic loads.

The wind excitation was modelled on the basis of the Kaimal spectrum, representing turbulent wind as a time-varying process composed of harmonic components with superimposed random disturbances. To assess the structural response, modal analysis was first conducted to determine the natural frequencies and vibration modes of the dome. This step was essential to evaluate the potential for resonance, as resonance occurs when the excitation frequencies of wind gusts coincide with the natural frequencies of the structure. Spectral analyses of simulated wind records for average wind speeds of 30 m/s, 35 m/s, and 40 m/s were performed using the fast Fourier transform (FFT). These analyses provided power spectra from which dominant wind frequencies – those with the highest amplitudes – were extracted and compared with the natural frequencies of the dome to assess resonance risk.

Dynamic response characteristics were then determined for each wind case. Time histories of displacements and accelerations were evaluated at the dome keystone, which represents a critical point in terms of global roof dynamics. Additionally, the variation of axial force in the most heavily stressed bar element was examined to assess the potential structural vulnerability. The results revealed how increasing average wind speed not only amplifies structural response but also shifts the likelihood of resonance, emphasizing the need for careful dynamic assessment under

non-standard wind conditions. The investigation built on the authors' earlier research [8–11], which demonstrated the necessity of including nonlinear geometric effects in roof analysis. In the present work, while geometric nonlinearity was considered to capture large displacements and stability effects, the material behaviour remained linear and governed by Hooke's law. This combination allows for realistic modelling of the structural behaviour of a roof under intense wind excitation without unnecessary complexity.

Overall, the study highlighted the importance of dynamic analysis in evaluating the safety and serviceability of lightweight, low-elevation bar roofs exposed to foehn winds. By combining advanced numerical simulations, spectral wind modelling, and modal analysis, the paper provides insight into resonance phenomena and structural response mechanisms that cannot be captured by conventional static wind load approaches. The findings contribute to improving the reliability of dome roof design in the regions where strong and gusty foehn winds may occur.

SPECTRAL ANALYSIS OF SIGNALS

In civil engineering, accurate assessment of the impact of dynamic interactions – particularly wind loads – on structures is crucial to ensuring their safety, durability, and comfort of use. One tool for analysing such interactions is the spectral analysis of time-based signals of wind force, pressure, displacement, and acceleration.

In wind engineering, modelling the turbulent components of wind speed is of particular importance. Among the models describing the distribution of turbulent energy as a function of frequency, the Kaimal spectrum [12, 13] is a key model – an empirical model that forms the basis of field experiments in American units. The Kaimal spectrum is recommended by standards [14, 15]. The power spectrum of the turbulent wind component, according to Kaimal, is the equation:

$$S_u(f) = \frac{\frac{4\sigma_u^2 L_u}{u_0}}{\left(1 + \frac{6fL_u}{u_0}\right)^{\frac{5}{3}}} \tag{1}$$

where: $S_u(f)$ – power spectrum of the wind component, σ – variance of turbulence in the component, L_u – turbulence integral scale length [m], u_0 – average wind speed [m/s], f – frequency [Hz].

The spectrum $S_u(f)$ indicate how much turbulent energy is present in each frequency band. Dynamic analyses use a wind model based on a Fourier series, representing the variation of wind speed over time as the sum of several simple sinusoidal waves (harmonic components). Each component has its own frequency, amplitude, and initial phase, and is responsible for a different "rhythm" of wind changes – one for slow fluctuations, the other for fast oscillations. A wind waveform that closely approximates the actual wind waveform is obtained by summing these values. To achieve a random waveform, each harmonic is assigned an independent phase $\varnothing_k \sim u(0.2\prod)$.

$$u'(t) = \sum_{k=1}^{N} A_k \cos\left(2\Pi f_k t + \emptyset_k\right) \tag{2}$$

where: A_k – amplitude determined from te Kaimal spectrum, $A_k = \sqrt{2S_u(f_k)\Delta f}$, $f_k = k\Delta f$ – subsequent discretization frequencies, $\varnothing_k$ - random phases.

The full time series is the sum of the mean value and turbulence:

$$u(t) = u_0 + u'(t) \tag{3}$$

Any time signal can be represented in the frequency domain using a Fourier transform. The authors used the FFT algorithm in their work. To determine how the signal energy is distributed as a function of frequency, power spectrum graphs were plotted for each signal. If the wind changes slowly, the load acts as a gentle "push" on the structure. If the wind changes at a frequency close to the natural frequency of the structure, resonance, i.e., significant vibration amplification, can occur. The wind speed spectrum allows prediction of the frequencies at which the structure will be most vulnerable. For the signals analysed in this work, the concentration of energy in the low-frequency range indicated the dominance of slowly varying components. In the work, the power spectra of the wind speed signal were calculated using Welch's method [16]. After determining the dominant wind load frequencies, the authors conducted a modal analysis of the structure.

MODAL ANALYSIS

Modal analysis is one of the basic tools used in structural dynamics to understand and predict how a structure will behave under the influence of vibrations. It is a dynamic analysis method that allows the identification of basic dynamic characteristics of a structure, such as natural frequencies (modal), vibration modes (modal shapes). Natural frequencies are the specific frequencies at which a structure tends to naturally vibrate when excited. Each structure has a range of such frequencies that are unique to its geometry, materials, and boundary conditions. Vibration modes are characteristic shapes that a structure takes when vibrating at a specific natural frequency. These modes show how different points of the structure move relative to each other. At the beginning of modal analysis, a mathematical model of the structure, which is based on finite element method (FEM) was created.

Schwedler dome is modelled as spatial frame. The bars are rigidly connected to each other at the nodes. Dome is supported in a pinned manner. Schwedler dome presented in the article is characterised by a strongly nonlinear static and dynamic response. The description of the analysed load cases together with a detailed static and strength analysis of the dome was published in the article [9]. Ignoring nonlinear effects leads to large computational errors. For this reason, the influence of axial forces S is taken into account:

$$\left[K_L + K_G(S) - \omega_i^2 M\right] w_i = 0 \tag{4}$$

where: K_L – linear stiffness matrix, $K_G(S)$ – the geometric stiffness matrix, M – the mass matrix, ω_i – the eigenfrequencies, w_i – the vector called the eigenvector of the i-th mode of vibration.

On the basis of the calculated natural frequencies and vibration modes, potential dynamic problems such as resonance can be identified. Resonance is a process in which the frequency of an external excitation approaches the natural frequency. This situation can lead to a significant increase in vibration amplitudes and possible damage to the structure. Modal analysis helps designers predict the behaviour of structures under earthquakes, high winds, or other dynamic loading. The analysis can be used to assess the performance of existing structures by comparing current vibration modes and frequencies with theoretical or historical values.

Articles [18–19] highlighted the issues related to monitoring bridge displacements, taking into account experimental and numerical studies. Furthermore, article [18] presented a preliminary proposal for a measurement system for monitoring the condition of existing and operated structures. The article presented the results of modal and numerical analysis. Article [19] considered structural health monitoring (SHM) strategies aimed at verifying the load-bearing capacity of the considered bridge. Measurements of the global response of the bridge are also included to prepare and validate the FEM model.

DIRECT INTEGRATION METHODS FOR EQUATIONS OF MOTION

Direct integration methods are numerical techniques employed to solve dynamic problems in which second-order differential equations describe the motion of mechanical systems. Unlike modal approaches, which reduce the number of degrees of freedom through eigenvalue decomposition, direct methods compute the system response directly in the time domain by advancing the solution step by step. Among the most widely used techniques are the Newmark method, Runge-Kutta schemes, and the Wilson-θ method.

Runge-Kutta methods form a class of single-step schemes, available in both explicit and implicit formulations [19–20]. They estimate the solution increment within a time step using weighted averages of the derivative function. The classical fourth-order Runge-Kutta (RK4) method is particularly popular, as it provides high accuracy by performing four derivative evaluations per step. These methods are especially effective for nonlinear problems, where linear-based approaches may fail. However, due to limited stability in stiff systems, small time steps are often required, which significantly increases computational cost.

The Wilson-θ method [21–22] extends the Newmark scheme with the introduction of the parameter θ (typically $\theta \geq 1.37$), which effectively advances the solution beyond the current time step by a fraction θ of the step size. This modification enhances stability, making the method unconditionally stable and efficient in suppressing high-frequency numerical oscillations. Nevertheless, this stability improvement comes at the expense of increased computational effort and the risk of introducing artificial damping, which may

distort the dynamic response if θ is not properly selected. The Newmark method [23–24] constitutes a family of time integration algorithms based on Taylor series approximations of velocity and displacement, governed by two control parameters. Their selection determines the numerical properties of the scheme, such as accuracy and stability. It was developed [25] by Nathan M. Newmark in 1959 and has since become a standard tool in structural dynamics, especially in solving the problems related to vibration and seismic analysis. Newmark's method is widely used in the analysis of engineering structures, especially in the analysis of the response to dynamic loads such as earthquakes, wind loads, and other dynamic excitations.

The Newmark, Runge-Kutta, and Wilson-θ methods exhibit distinct characteristics in terms of stability, accuracy, and computational efficiency. Runge–Kutta methods deliver superior accuracy for small time steps (particularly in nonlinear analyses), while the Wilson-θ method ensures unconditional stability with effective suppression of spurious high-frequency modes. The authors selected the Newmark method due to its favourable balance between computational efficiency and numerical stability. By employing this algorithm, it was possible to obtain reliable time-domain responses of the system, while significantly reducing computational costs compared to higher-order or more complex integration schemes. Due to its stability and flexibility, Newmark method is often used in finite element analysis software. Basic equation of motion can be written as:

$$M\ddot{q} + C\dot{q} + (K_L + K_G(S))q = P \tag{5}$$

where: C is the damping matrix, q is the vector of nodal displacements, P is the vector of nodal load. The following initial conditions are assumed:

$$q(0) = q_0 \text{ and } \dot{q}(0) = \dot{q}_0 \tag{6}$$

The essence of the method is to abandon the solutions in a continuous set of time variables and to limit oneself to the solutions for discrete time division. This procedure leads from a system of ordinary differential equations to algebraic equations. The obtained systems of equations form a recursive sequence, which allows for determining solutions at the next moment, depending on solutions at previous moments (a discrete set of points ti on the time axis with the integration step $h = ti+1 - ti$). Then, the representation of the solution of the equation will be the set of vectors displacements and velocities. The velocities and displacements expand the function into a Taylor series:

$$\dot{q}_{i+1} = \dot{q}_i + h\ddot{q}_i + \frac{1}{2}h^2\dddot{q}_i + \cdots \tag{7}$$

$$q_{i+1} = q_i + h\dot{q}_i + \frac{1}{2}h^2\ddot{q}_i + \frac{1}{6}h^3\dddot{q}_i + \cdots \tag{8}$$

The formulas (7) and (8) are modified as leaving terms of the second order at most. The remaining terms of the Taylor expansion with arithmetic means for velocities and weighted averages for displacements:

$$\dot{q}_{i+1} = \dot{q}_i + \frac{1}{2}h\ddot{q}_i + \frac{1}{2}h\ddot{q}_{i+1} \tag{9}$$

$$q_{i+1} = q_i + h\dot{q}_i + (\frac{1}{2}-\beta)\, h^2\ddot{q}_i + \beta h^2\ddot{q}_{i+1} \tag{10}$$

where: parameter $\beta \in <0; \frac{1}{2}>$.

From the formula (10), we obtain:

$$\ddot{q}_{i+1} = \frac{1}{\beta h^2}[q_{i+1} - q_i - h\dot{q}_i - (\frac{1}{2}-\beta)\, h^2\ddot{q}_i] \tag{11}$$

Newmark's method is an implicit method. The solutions at time i+1 are obtained by satisfying the collocation conditions at time i+1:

$$M\ddot{q}_{i+1} + C\dot{q}_{i+1} + (K_L + K_G(S))q_{i+1} = P_{i+1} \tag{12}$$

At the starting moment, the vector $\ddot{q}_0$ must be calculated by writing the collocation equation for time t = 0.

$$\ddot{q}_0 = M^{-1}(P_0 - C\dot{q}_0 - (K_L + K_G(S))q_0) \tag{13}$$

RESULTS AND DISCUSSION

Wind signal analysis

In thus work the authors aimed to show the signal in various aspects. The amplitude spectrum, power spectrum, and RMS spectrum are three related but distinct ways of describing a signal in the frequency domain. Amplitude spectrum represents the distribution of signal amplitudes as a function of frequency. It directly describes the magnitude of individual harmonic components contained in the signal. In the case of wind velocity, it indicates how strong the velocity fluctuations are at a given frequency. The typical unit is m/s.

Power spectrum represents the distribution of the signal energy as a function of frequency. It is calculated as the squared modulus of the

amplitude spectrum, normalised with respect to the number of samples and/or bandwidth. The power spectrum indicates what fraction of the total signal energy is associated with particular frequency bands. For wind velocity signals, the units are usually m²/s² or (m²/s²)/Hz when expressed as power spectral density (PSD).

RMS spectrum (Root Mean Square spectrum) is an intermediate form of representation derived from the power spectrum. It is obtained by calculating the square root of the product of the power spectral density and the analysed frequency bandwidth. The RMS spectrum provides information on the effective value of the signal within individual frequency bands. It is therefore a measure of the "actual strength" of the signal in a given range, and its unit remains the same as for the original signal.

Signals for three average wind speeds: u_0 = 30 m/s (Figure 1a), u_0 = 35 m/s (Figure 2a), and u_0 = 40 m/s (Figure 3a) were generated using the Kaimal spectrum. For each case, the RMS spectrum for three different variants of the number of samples was also included (Figures 1b, 2b, 3b). Fast Fourier transform and Welch's method were used to estimate the power density spectrum (Figures 1c, 2c, 3c) and amplitude (Figures 1d, 2d, 3d). For the power density and amplitude spectra, the horizontal axis shows the frequency in Hz, and the vertical axis shows the power spectral density (on a linear scale), which shows how the signal energy is distributed in the frequency domain.

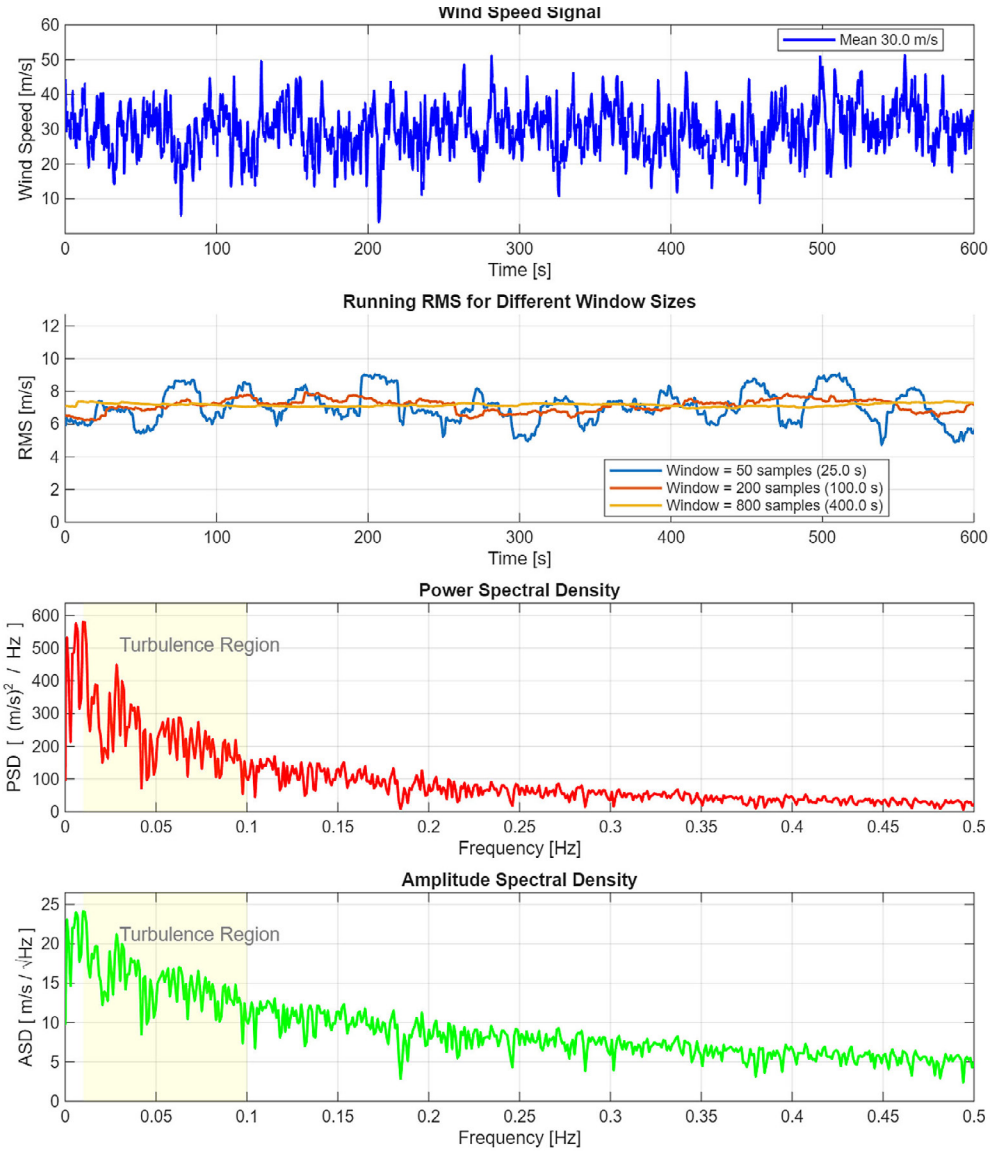

Figure 1. Results for average wind speed u_0 = 30 m/s: (a) wind signal analysis – Kaimal Spectrum, (b) RMS, (c) power spectral density, (d) amplitude spectral density

In the context of turbulence spectra, the term "dominant frequency" refers to the frequency at which the power spectral density (PSD) reaches its maximum. This frequency is associated with the highest kinetic energy of wind speed fluctuations. For all the analysed cases, most of the signal energy is concentrated at low frequencies, below ~0.1 Hz, which is typical for wind signals dominated by slow fluctuations. Around 0.2–0.3 Hz, the spectrum drops significantly, indicating the absence of substantial high-frequency components (rapid wind speed changes). In each case, the highest power occurs at the lowest frequencies, below 0.01 Hz. The PSD magnitude increases with rising wind speed – from approximately 550 m²/s²/Hz at u_0 = 30 m/s to about 730 m²/s²/Hz at u_0 = 40 m/s. All three spectra exhibit the characteristic shape of the Kaimal spectrum: a steep rise at very low frequencies, a distinct peak, and a subsequent decay following the $f^{-5/3}$ relationship in the high-frequency range (the so-called "inertial subrange" or "isotropic similarity"). A similar trend is observed for the power amplitude, indicating that the signal primarily contains low-frequency components, typical of wind speed fluctuations. The main factor differentiating the spectra is the nominal wind speed. An increase in average wind speed leads to:

- a higher signal magnitude in the time domain,
- greater amplitudes of turbulent fluctuations (i.e., higher signal variance),
- increased overall power and spectral amplitude across the entire frequency range.

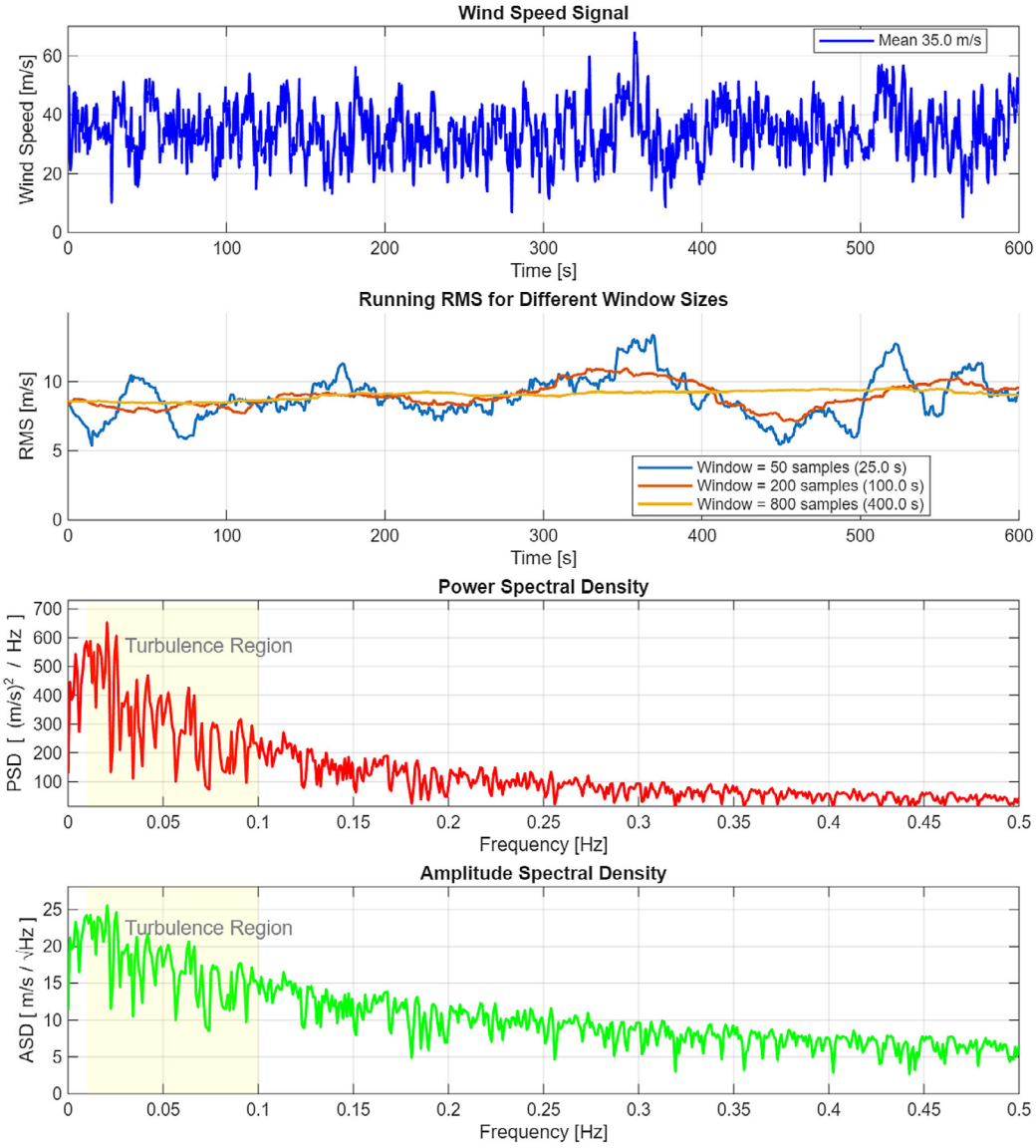

Figure 2. Results for average wind speed u_0 = 35 m/s: (a) wind signal analysis – Kaimal Spectrum, (b) RMS, (c) power spectral density, (d) amplitude spectral density

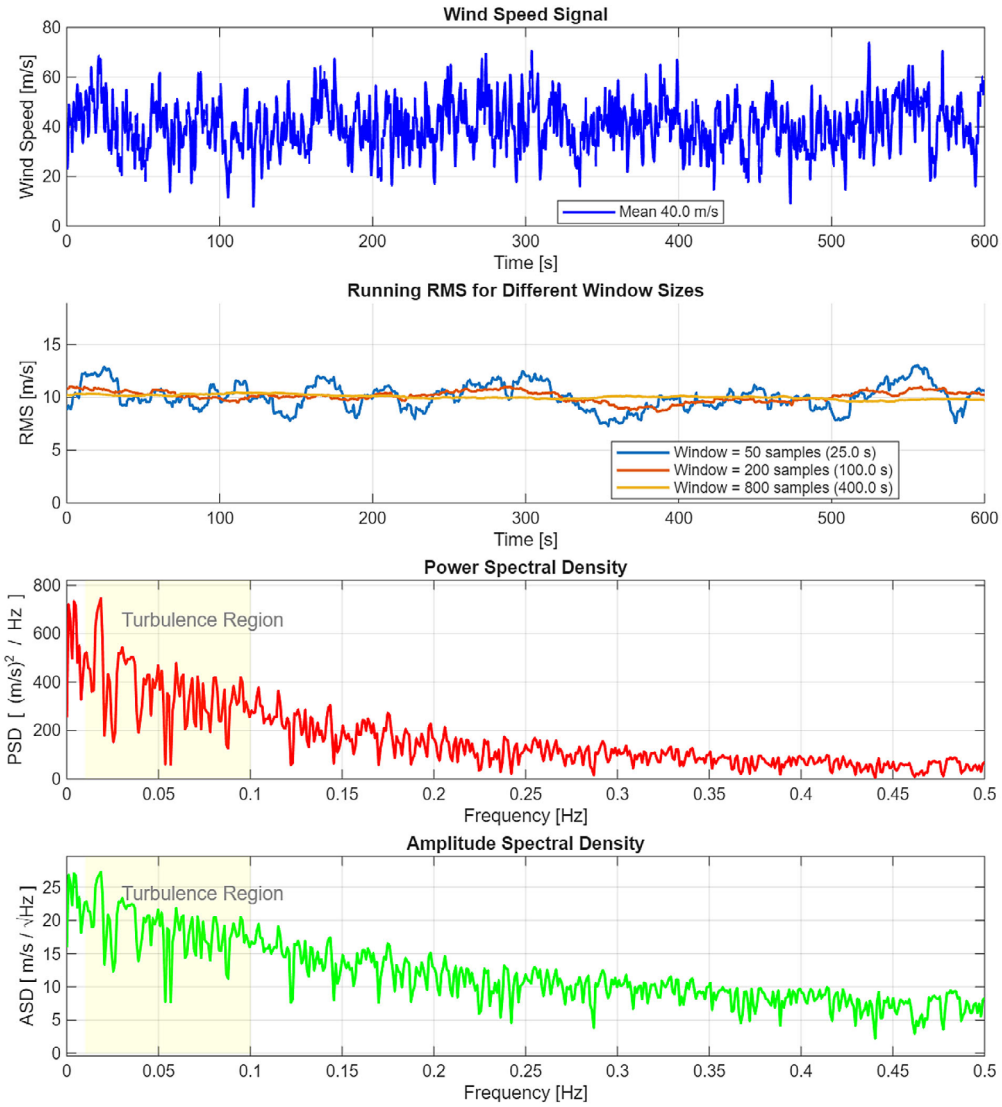

Figure 3. Results for average wind speed u_0 = 40 m/s. (a) Wind signal analysis – Kaimal Spectrum, (b) RMS, (c) power spectral density, (d) amplitude spectral density

The comparison of spectra for the three wind speeds clearly illustrates the fundamental principles of turbulence modelling using the Kaimal spectrum. As the mean wind speed increases, turbulence becomes stronger and more dynamic, and the total energy rises. Despite these differences, the relative spectral shape remains similar, which is a key property of a robust stochastic model. The shift of the spectrum indicates that the relative distribution of energy across turbulence scales is preserved, but "stretches" toward higher frequencies as the wind speed increases – stronger winds produce faster and more energetic gusts that carry the most energy. Therefore, spectral analysis cannot rely on a fixed dominant frequency. The design of wind-exposed structures must account for the full range of possible operating wind speeds to ensure that resonance does not occur under any of these conditions. This phenomenon has significant engineering implications. Structures such as roofs, towers, bridges, and wind turbine blades have fixed natural vibration frequencies. As wind speed increases, so does the likelihood that the dominant excitation frequency (derived from the turbulence spectrum) approaches or coincides with the natural frequency of the structure. This may lead to resonance—a dynamic amplification of vibrations that drastically increases loading and can cause fatigue damage or even structural failure.

Numerical model of the structure

This paper considered a Schwedler dome with a diameter of 25 meters and a height of 1 meter, mounted on a reinforced concrete ring topped by 16

reinforced concrete columns, each 10 meters high. The dome consists of 81 nodes and 224 rods (Figure 4). The dome is modelled using steel tubes with a Young's modulus E = 210 GPa, a yield strength fy = 355 MPa, and a Poisson's ratio v = 0.3. The structure was modelled as a spatial frame (assuming rigid connections at the nodes).Three groups of rods were considered for the structural design: meridians, parallels, and diagonals. The meridians were modelled from RO127x8.8 circular steel tubes, the parallels from RO273x8.8 circular tubes, and the diagonals from RO82.5x6.3. The meridians have a uniform length of 2.511 m, while the parallels have different lengths of 4.877 m, 3.908 m, 2.934 m, 1.958 m, and 0.979 m, respectively. The roof covering is made of steel tubes and glass panels.

Dynamic response analysis of a dome structure under wind loading

The modal analysis performed showed that the first mode of natural vibrations is antisymmetric. The structure tends to lose global stability (taking the entire structure into account simultaneously). For the discussed Schwedler dome, the value of the first five natural frequencies is: 3.45 Hz, 3.45 Hz, 55.72 Hz, 5.75 Hz, 5.75 Hz, respectively. The dominant spectral energy of the foehn wind is concentrated in very low frequencies (on the order of 10^{-3}–10^{-1} Hz), which means that the main gust components will not resonate with the modal frequencies of the dome (3.45 Hz and 5.72 Hz). In practice, if the structure contains elements with characteristic dimensions on the order of several tens of centimetres to a meter, then under realistic foehn wind speeds (ranging from several to several tens of meters per second), vortex shedding may generate frequencies in the range of 3–6 Hz, potentially coinciding with the modal frequencies of the dome. This phenomenon, however, was not analysed in the present work.

In the analysis, the dimensionless damping coefficient γ for steel structures was assumed to be 0.02. The dimensionless constants κ and μ in the Rayleigh model were assumed to obtain a critical damping of 1%.

The damping matrix C is described as:

$$C = \mu \cdot M + \kappa(K_L + K_G(S)) \tag{14}$$

The values of the parameters μ and κ determined on the basis of the first two significant vibration frequencies are κ = 0.0003, μ = 0.2702.

The wind load was assumed as shown in Figures 1–3. Figures 5–7 present the dynamic responses of displacement, force, and acceleration at given wind speeds of u_0 = 30 m/s, u_0 = 35 m/s, and u_0 = 40 m/s. Analysis of the time histories of vertical displacements of the keystone demonstrated a clear effect of wind speed on the amplitude and nature of the dynamic response of the structure. As wind speed increased, the displacement amplitude increased nonlinearly (from approximately 12 mm for u_0 = 30 m/s to approximately 21 mm for u_0 = 40 m/s), which results from the quadratic relationship between aerodynamic forces and flow velocity. In each case, maximum displacements were reached in the initial phase (less than 2–3 seconds) and then gradually diminished due to structural and aerodynamic damping. For each case, there is a rapid amplitude decay in the first seconds (0–5 s), suggesting relatively good damping properties of

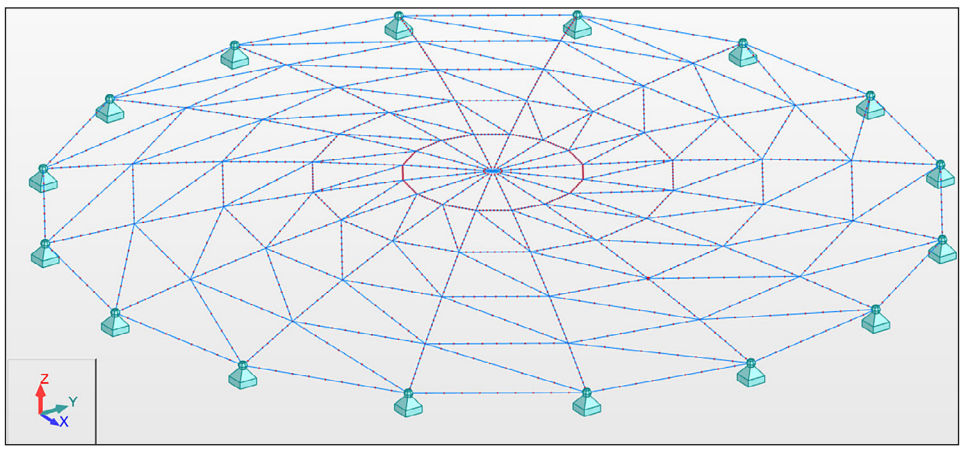

Figure 4. Schwedler dome geometry

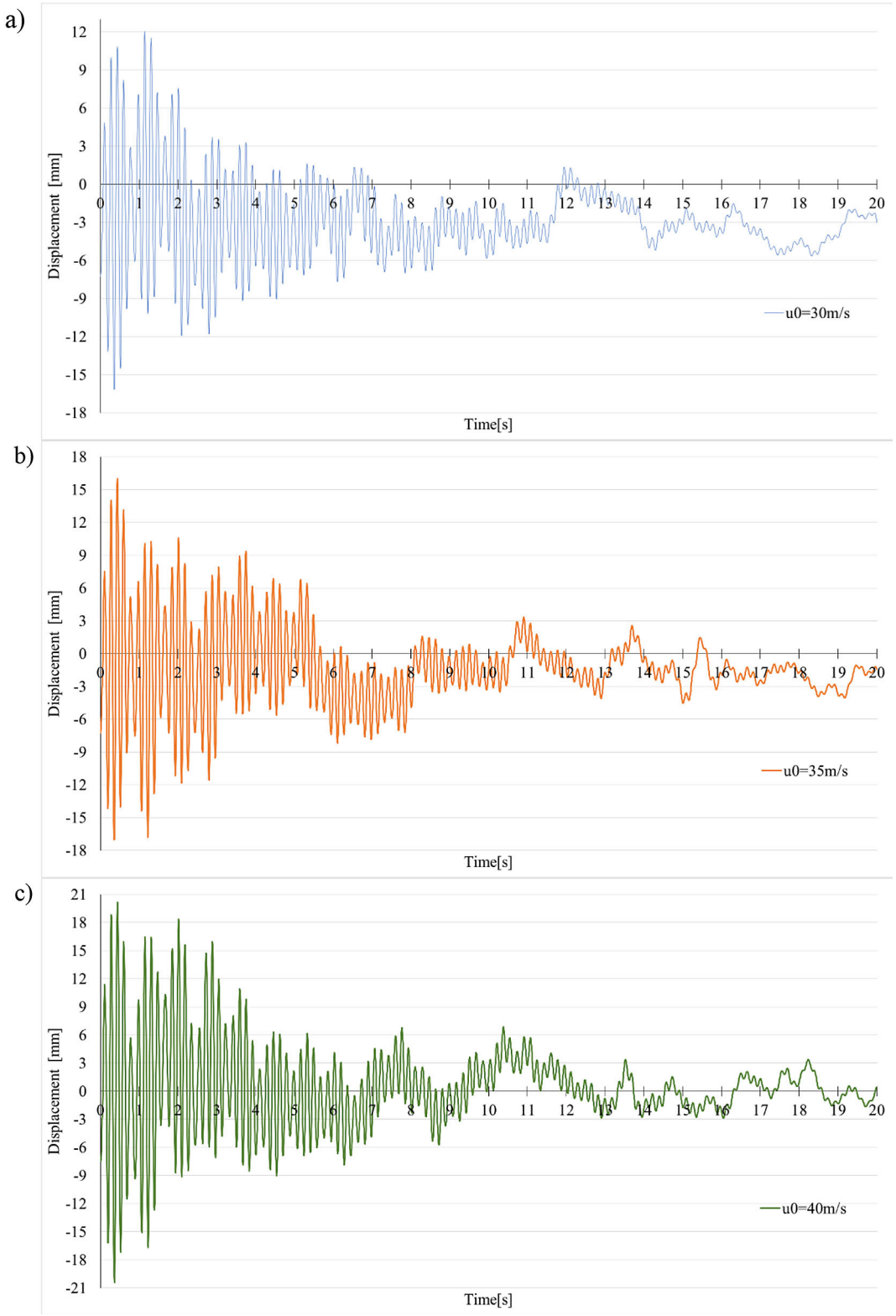

Figure 5. Dynamic response of the structure – displacement, a) $u_0 = 30$ m/s, b) $u_0 = 35$ m/s, c) $u_0 = 40$ m/s

the structure. The axial force in the most stressed member undergoes cyclic changes from tension in the leeward direction to periodic compression in the windward direction, with the range of change increasing with wind speed in a manner that is almost quadratic. The force values range from approximately 190 kN of compressive force to approximately 160 kN of tensile force for a wind speed of $u_0 = 30$ m/s, and from approximately 200 kN of compressive force to approximately

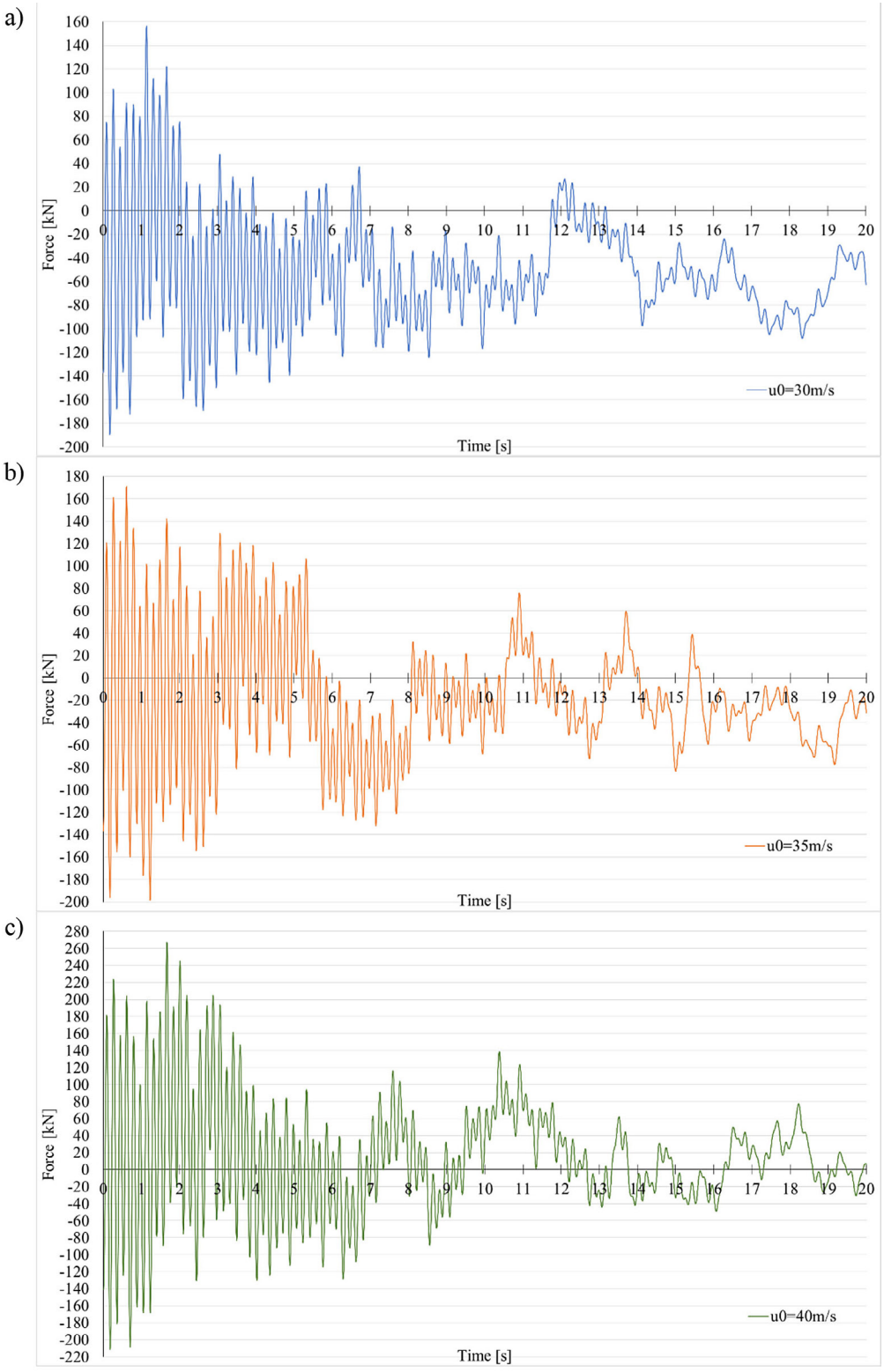

Figure 6. Dynamic response of the structure – Force: a) u_0 = 30 m/s, b) u_0 = 35 m/s, c) u_0 = 40 m/s

170 kN of tensile force for a wind speed of u_0 = 35 m/s. For an average wind speed of u_0 = 40 m/s, the range changes from approximately 210 kN of compressive force to approximately 270 kN of tensile force. At the highest speed, it was observed that the maximum tensile values approach the ultimate limits of the load-bearing capacity, and during compression, the risk of local buckling occurs, especially in slender members. Furthermore, an increased number of cycles with

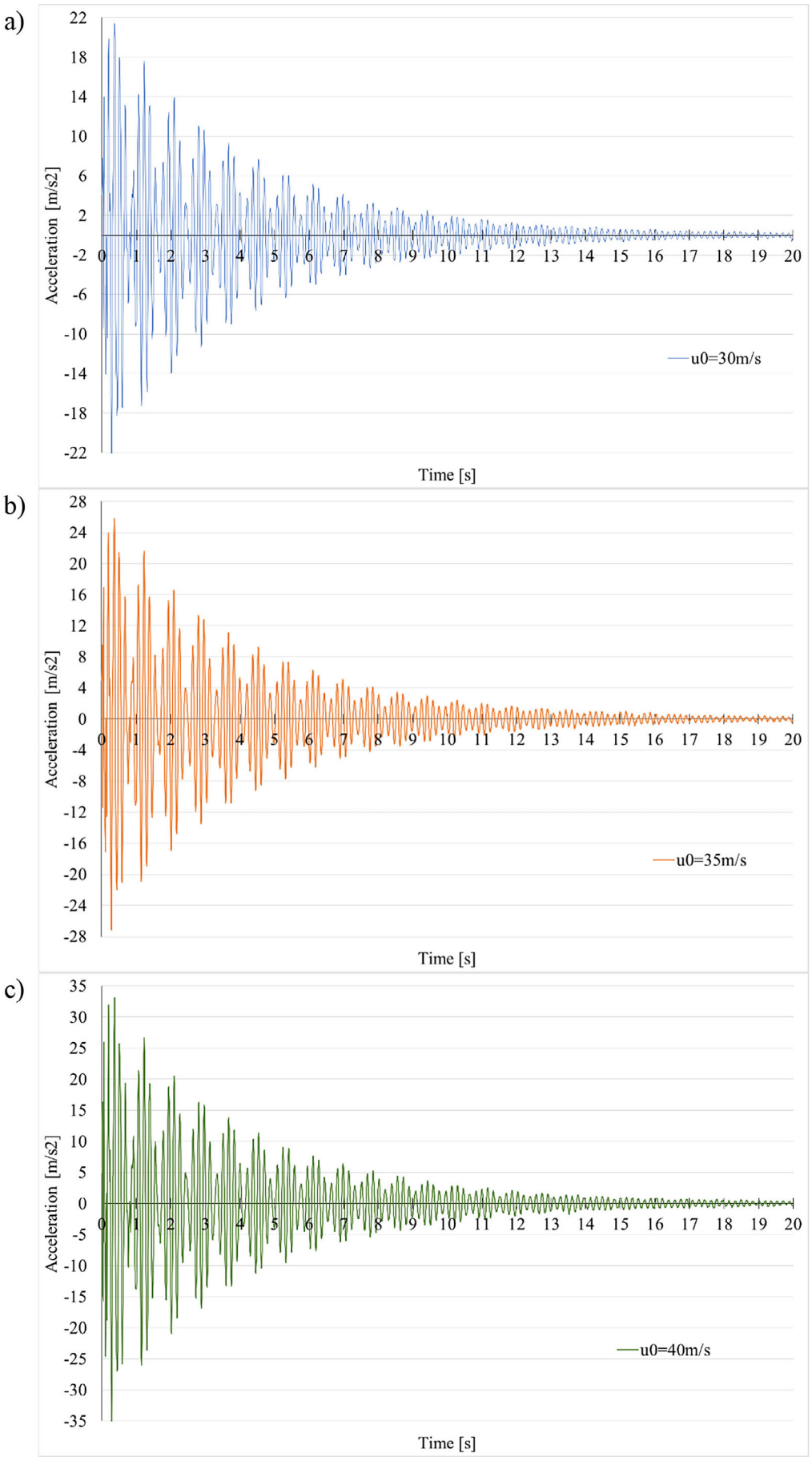

Figure 7. Dynamic response of the structure – Acceleration, (a) u_0 = 30 m/s, (b) u_0 = 35 m/s, (c) u_0 = 40 m/s

increasing amplitude can generate significant fatigue loads. Acceleration recorded at the keystone showed an even stronger dependence on wind speed than displacement. The values of maximum accelerations for u_0 = 30 m/s reach 22 m/s^2, for u_0 = 35 m/s they reach 27 m/s^2 and for u_0 = 40 m/s they reach 35 m/s^2. Increasing flow velocity caused a sudden increase in the maximum acceleration values, which is a natural consequence of the relationship between acceleration and the second derivative of displacement.

Additionally, the effect of the γ coefficient on the change in displacement over time was investigated. Simulations were performed for γ values ranging from 0.01 to 0.025, which corresponds to typical values for steel structures (Figure 8). The obtained results indicate significant differences in the maximum displacement values. These values range from approximately 12.5 mm for γ = 0.01 to approximately 9 mm for γ = 0.025. Additionally, differences in the quality of the graph are also noticeable, with γ = 0.01 being significantly more 'uneven' than γ = 0.025. These values clearly indicate the influence of the γ coefficient on the structure damping.

DISCUSSION OF RESULTS AND PRACTICAL CONCLUSIONS

A foehn is a gusty, short-lived, typically dry, and warm wind. In the Tatra Mountains, it occurs seasonally, lasting from a dozen to even several dozen days per year, depending on the applied criteria. Under such conditions, a fatigue analysis of the structure may be necessary. Detailed analyses addressing this issue are planned for later stages of the research. Further investigation and a more comprehensive analysis are required to develop standard design recommendations. However, based on the authors' experience and previous studies, several conclusions can already be drawn. Dynamic analyses should be considered when peak wind gusts exceeding 20 m/s are expected in the analysed region. When the average gust speed exceeds 30 m/s, a full dynamic structural analysis is recommended, including verification of potential resonance effects. This approach complies with EN 1991-1-4, which specifies that if a structure is capable of resonating with gust energy, dynamic effects must be taken into account. Therefore, if the excitation-to-natural frequency ratio indicates possible resonance coupling (i.e., the main natural frequency of the structure falls within the typical gust energy range of 0.1–2 Hz), a modal analysis with spectral excitation should be performed.

For roofing systems exposed to strong gusts, it is advisable to consider several analysis variants depending on the wind conditions. In the cases of short-term gusts (> 20 m/s), structural deformation and vibration should be verified with respect to user comfort and the proper functioning of roof components – specifically connections, joints, and seals (bolts, gaskets, etc.). In such cases, a modal analysis that includes an increased gust coefficient may be sufficient.

When prolonged gusts are expected (e.g., more than 10 days with average gusts above 20 m/s, or shorter periods with higher speeds), fatigue verification of critical components (nodes, joints, thin-walled profiles, etc.) becomes necessary. Since the number of days with strong gusts is often uncertain, adopting a conservative estimate (e.g., at least 20 days) is recommended.

A detailed fatigue analysis requires precise structural and meteorological data. One possible approach involves temporal (spectral) analysis of the structure response. For preliminary assessments, the Palmgren–Miner rule can be applied to estimate the number of years after which fatigue failure risk becomes significant. The number of loading cycles can be approximated by comparing the average number of small gust cycles per year with the expected number of gusts, depending on component classification.

If modal and spectral analyses indicate low damping and a significant increase in amplitude near frequencies associated with foehn winds, the use of damping devices is recommended. Damping devices are used, among others, in high-rise structures and bridges [26, 27]. Regions frequently affected by strong foehn gusts may also experience numerous smaller gust cycles of lower power but higher intensity; therefore, including dampers at the design and construction stages represents a prudent, conservative approach.

The results indicate that the dynamic response of the dome is highly sensitive to increasing wind speeds. The most critical parameters include keystone accelerations (relevant to user comfort and equipment protection) and axial force ranges in key members (relevant to load-bearing capacity and fatigue life). The tests did not reveal a single dominant resonance; the observed response suggests the interaction of multiple structural modes. At higher wind speeds, irregular fluctuations in displacement and acceleration amplitudes were observed,

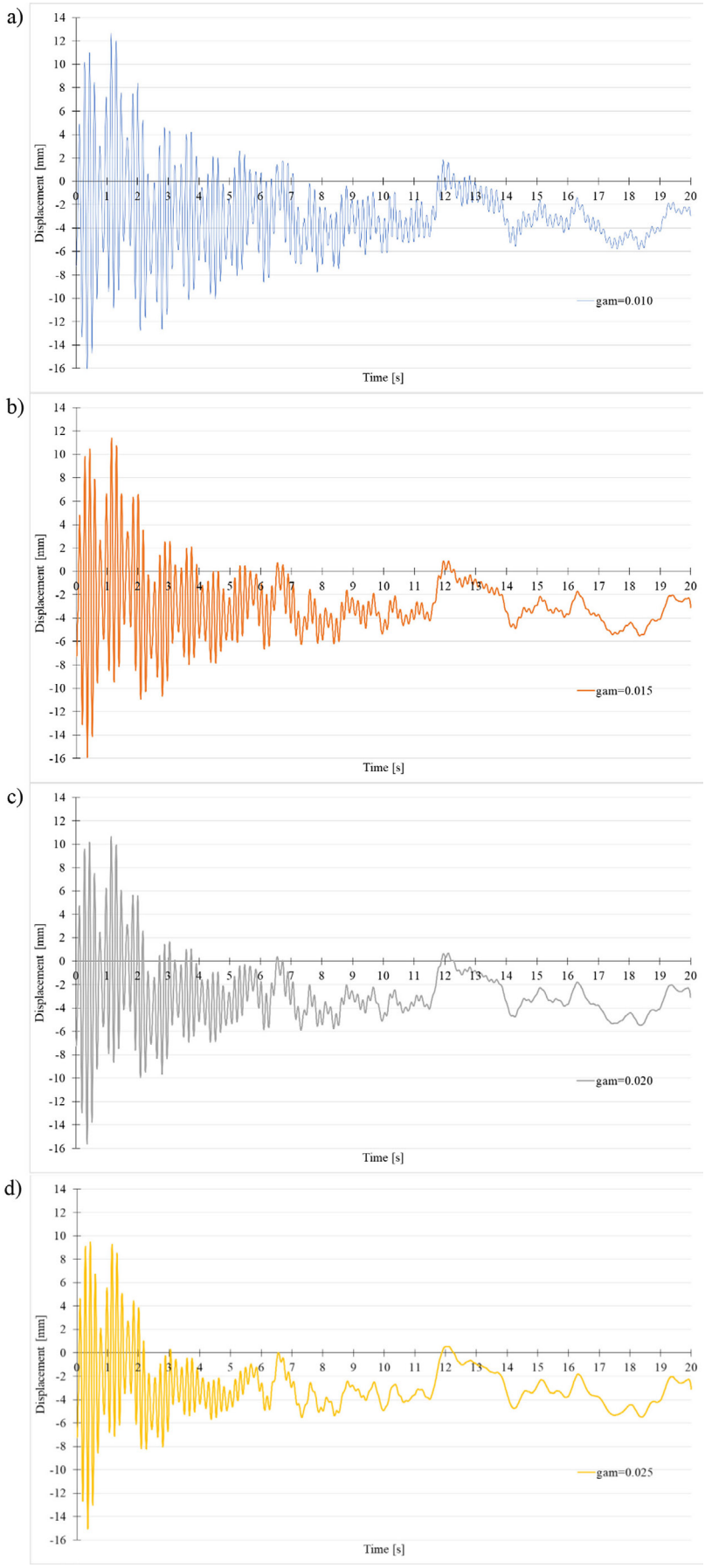

Figure 8. Root mean square spectrum – displacement, (a) $\gamma = 0.01$, (b) $\gamma = 0.015$, (c) $\gamma = 0.02$, (d) $\gamma = 0.025$

possibly indicating amplitude modulation (beating). Maximum deflections and accelerations were found to increase approximately quadratically with wind speed, which should be considered when extrapolating results to design-level conditions.

REFERENCES

1. Twardosz R. Circulation features of days with foehn wind in the Tatra region. Przegl Geogr. 2010;82(1):95–112.
2. Lorenc H. Climate Atlas of Poland. Warsaw: Institute of Meteorology and Water Management (IMGW); 2005.
3. Sun Y, Qiu Y, Wu Y. Modeling of wind pressure spectra on spherical domes. Int J Space Struct. 2013;28(2):87–100.
4. Ren Q, Yang. The analysis of wind vibration coefficient of long-span dome structures with different thickness. In: Earth and Space 2012.
5. Tavares da Silva F. Parametric 2D wind loading on hemispheric dome structures. In: SIGraDi 2016: XX Congress of the Iberoamerican Society of Digital Graphics; 2016; Argentina.
6. Szmit R. Geometry design and structural analysis of steel single-layer geodesic domes. In: 2017 Baltic Geodetic Congress (BGC Geomatics); 2017; Gdańsk.
7. Khosrowjerdi M, Sarkardeh H, Kioumarsi M. Effect of wind load on different heritage dome buildings. Eur Phys J Plus. 2021;136(11).
8. Radoń U, Zabojszcza P, Sokol M. The influence of dome geometry on the results of modal and buckling analysis. Appl Sci. 2023;13:2729.
9. Opatowicz D, Radoń U, Zabojszcza P. Assessment of the effect of wind load on the load capacity of a single-layer bar dome. Buildings. 2020;10:179.
10. Zabojszcza P, Radoń U. Effect of increased density of nodes in geodesic dome on its critical load capacity. IOP Conf Ser Mater Sci Eng. 2019;471:052051.
11. Zabojszcza P, Radoń U. The impact of node location imperfections on the reliability of single-layer steel domes. Appl Sci. 2019;9:2742.
12. Kaimal JC, Wyngaard JC, Izumi Y, Coté OR. Spectral characteristics of surface-layer turbulence. Q J R Meteorol Soc. 1972.
13. Kaimal JC. Turbulence spectra, length scales and structure parameters in the stable surface layer. Bound Layer Meteorol. 1973.
14. European Committee for Standardization. EN 1991-1-4: Eurocode 1: Actions on structures – Part 1-4: Wind actions. Brussels: CEN; 2005.
15. American Society of Civil Engineers. ASCE/SEI 7-22: Minimum design loads and associated criteria for buildings and other structures. Reston, VA: ASCE; 2022.
16. Welch PD. The use of fast Fourier transform for the estimation of power spectra: A method based on time averaging over short, modified periodograms. IEEE Trans Audio Electroacoust. 1967.
17. Venglár M, Sokol M. Case study: The Harbor Bridge in Bratislava. Struct Concr. 2020;21:2736–48.
18. Sokol M, Venglár M, Lamperová K, Márföldi M. Performance assessment of a renovated precast concrete bridge using static and dynamic tests. Appl Sci. 2020;10(17):5904.
19. Self-Adjusting Multi-Rate Runge-Kutta Methods: Analysis and Efficient Implementation in An Open Source Framework, 2025.
20. Stephen J. Walters, Ross J. Turner, Lawrence K. Forbes A comparison of explicit Runge–Kutta methods, 2022.
21. Bathe KJ, Wilson, EL. Stability and accuracy analysis of direct integration methods, 1972.
22. Wilson EL, Farhoomand I, Bathe KJ. Nonlinear dynamic analysis of complex structures, 1973.
23. A Newmark space-time formulation in structural dynamics, 2021.
24. Improving the accuracy of the Newmark method through backward error analysis, Donát M. Takács, Tamás Fülöp, 2024.
25. Newmark NM. A method of computation for structural dynamics. J Eng Mech Div. 1959;85(3):67–94.
26. El Ouardani A, Tbatou T. Seismic isolators layout optimization using genetic algorithm within the Pymoo framework, Civil Engineering Journal, 2024;10(8).
27. Wang Z, Hu J, Jing W, Zhang W. Vibration control of corrugated steel web box girder bridge with friction pendulum isolation, Civil Engineering Journal, 2024;10(10).